Imbalance Mechanism and Balancing Control of DC Voltages in a Transformerless Series Injector Based on Paralleled H-Bridge Converters for AC Impedance Measurement

Zeng Liu, *Member, IEEE*, Igor Cvetkovic, *Member, IEEE*, Zhiyu Shen, *Member, IEEE*, Dushan Boroyevich, *Fellow, IEEE*, Rolando Burgos, *Member, IEEE*, and Jinjun Liu, *Fellow, IEEE*

***Abstract*—Small-signal stability of ac power systems is able to be assessed by measuring their terminal impedance, and a transformerless series injector is very attractive for wideband measurement of load impedances. A typical implementation of the transformerless series injector is paralleled H-bridge (PHB) converters, where dc voltage imbalance will occur when system current magnitude is larger than a critical point, and thus the operation region of the series injector is seriously restricted. To address this issue, this paper presents a deep analysis on the mechanism behind dc voltage imbalance for PHB-based series injector, and it is revealed that a positive feedback exists in the dc voltage balancing loop under high system current magnitude. Then an enhanced control scheme is proposed to balance dc voltages in full system current range, where a reactive component is injected in the output voltage while reactive circuiting current is introduced among H-bridge converters for redistributing active power. Furthermore, the system behavior with the proposed scheme is comprehensively analyzed and the reference design for the injected reactive component magnitude in the output voltage is offered. Finally, the imbalance mechanism and the proposed scheme are validated by simulation and experimental results.**

***Index Terms*—DC voltage balancing control, impedance measurement, paralleled H-bridge (PHB) converters, series injector, small-signal stability.**

Manuscript received July 28, 2018; revised September 24, 2018; accepted October 29, 2018. Date of publication November 12, 2018; date of current version May 22, 2019. This work was supported in part by the National Natural Science Foundation of China under Grants 51777160 and 51437007, and in part by the Power Electronics Science and Education Development Program of Delta Group under Grant DREG2018003. This paper was presented in part at the 33rd Annual IEEE Applied Power Electronics Conference and Exposition, San Antonio, TX, USA, Mar. 4–8, 2018. Recommended for publication by Associate Editor H. S. Krishnamoorthy.

Z. Liu and J. Liu are with the State Key Lab of Electrical Insulation and Power Equipment, School of Electrical Engineering, Xi'an Jiaotong University, Xi'an, Shaanxi 710049, China (e-mail:

current magnitude reaches and exceeds a critical point, which is much less than the designed current rating. Consequently, the PHB controlled by the existing scheme is just able to operate under the low system current magnitude condition, and the capability of impedance measurement is seriously limited.

To tackle the aforementioned issue, this paper presents a deep analysis on the mechanism behind dc voltage imbalance for PHB based series injector with the conventional control scheme and then proposes an enhanced control scheme to balance dc voltages in full system current range. Compared to existing publications [14], [15], the contribution of this paper can be summarized as below. At the beginning, the active power flow of single H-bridge converter is modeled, including the power losses of the filter inductor and the power semiconductor devices, and then the derivative of the dc power with respect to the inductor current magnitude is derived. It is revealed that this derivative turns to be negative when the operation point of the inductor current magnitude increases to a critical point where the resistive power losses introduced by the inductor as well as the power semiconductor devices just equal to the active power flowing into the dc capacitor, and thus the dc voltage balancing loop will be changed from negative feedback to positive feedback. Consequently, these dc voltages will not be balanced any more when the system current magnitude exceeds a corresponding value in the PHB-based series injector. Furthermore, an enhanced control scheme is proposed to extend the operation region of the PHB-based series injector, where a reactive component of the inductor current is trimmed instead of the active component in the conventional scheme [14], and the reactive component is injected into the output voltage. Thus then an interaction between the reactive components of the inductor currents and the reactive component of the output voltage is able to redistribute the active power flows among H-bridge converters to balance their dc voltages. Since the reactive component of the inductor current is adopted, dc voltage balancing is not dependent of system current anymore, and the series injector is able to operate in full system current range. Finally, the derivative of the dc power with respect to the reactive component magnitude of inductor current is investigated for each H-bridge converter, and then it is observed that the dc voltage will always be balanced when a proper reactive component magnitude of the output voltage is introduced, which is mainly dependent of the parameter variances among H-bridge converters and the maximum system current magnitude. And thus a guideline for designing the reactive component magnitude of the output voltage is offered.

The rest of this paper is arranged as follow. The system configuration of PHB-based series injector is introduced in Section II. Section III presents the imbalance mechanism of the dc voltages in PHB. The enhanced control scheme is proposed in Section IV. Section V gives the analysis and design for the proposed scheme. Section VI verifies theoretical analysis by simulation and experimental results. Finally, the conclusions are remarked in Section VII.

II. System Configuration

Fig. 1 shows a typical configuration of impedance measurement using a transformerless series injector for a three-phase ac power system divided into the source subsystem and the load subsystem, whose operation principle is presented in [14]. The series injector is inserted into phase A for injecting perturbation voltage to the system under measurement, while terminal voltages and currents of source and load are measured and processed for computing their impedances $\mathbf{Z}_{Sdq}$ and $\mathbf{Z}_{Ldq}$.

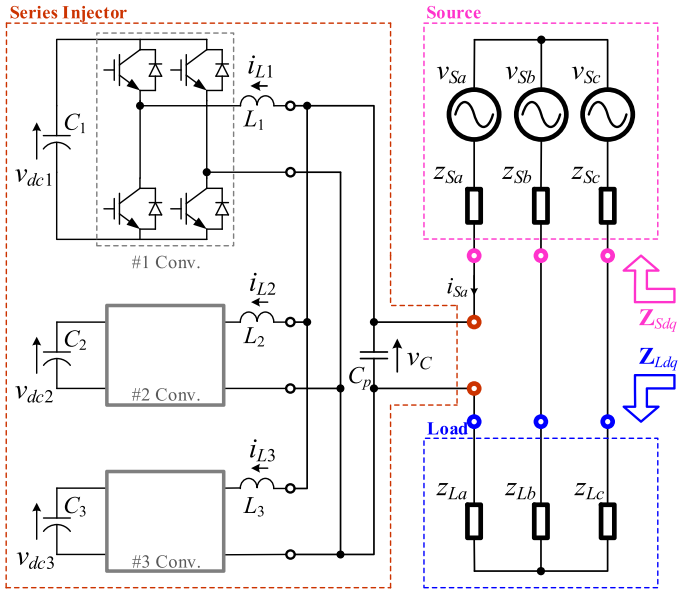

Fig. 1. Power stage of the impedance measurement setup for three-phase ac power system using a transformerless series injector based on three PHB converters.

In the series injector, the number of H-bridge converters N is set to 3 in this paper for simplification since the dc voltage balance characteristic is less dependent of N. Within each H-bridge converter, there are four IGBTs with anti-parallel diodes and an inductor L_k $(k = 1, \ldots, N)$. Their ac sides are paralleled together through the inductor L_k, while there is just a floating capacitor C_k on their dc sides for maintaining the dc voltage v_{dck}. Besides, an ac capacitor C_p is used to buffer the system current i_{Sa}. In the PHB-based series injector operating normally, perturbation voltage at given frequency is generated on the ac capacitor C_p, and system current i_{Sa} is equally shared among H-bridge converters while their dc voltages v_{dck} are balance and follow the voltage reference.

III. Imbalance Mechanism of DC Voltages in PHB With Existing Control Scheme

A. Description of Existing Control Scheme

For the PHB-based series injector, there are four control targets, which are as follows:

1) Average dc voltage regulation;
2) Perturbation voltage generation;
3) DC voltages balancing;
4) System current sharing among H-bridge converters.

To achieve these goals, dc voltages v_{dck}, inductor currents i_{Lk}, output voltage v_C, and system current i_{Sa} are sensed, and then processed by the control block diagram presented in Fig. 2, and eventually three duty cycle d_k are obtained, which are used to generate control signals for the IGBTs in corresponding

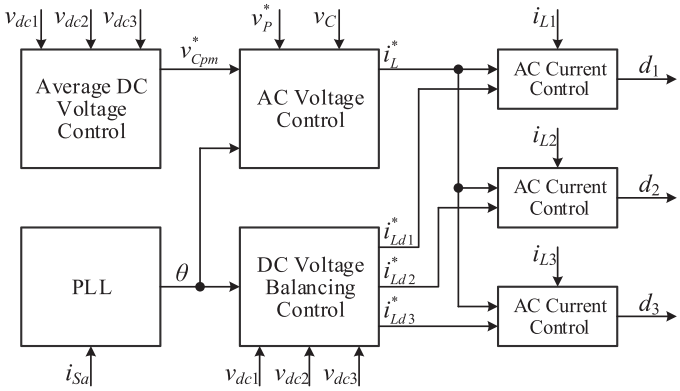

Fig. 2. Overall control block diagram for the series injector based on three PHB converters.

H-bridge converters by pulsewidth modulators. As shown in Fig. 2, existing control scheme is composed by an average dc voltage control, an ac voltage control, a phase-locked loop (PLL), a dc voltage balancing control, and three ac current controls.

The first control target is achieved by the average dc voltage control, whose inner structure is presented in Fig. 3(a). The average value of the dc voltages $\overline{v_{dc}}$ is first calculated out, and then compared with the dc voltage reference v_{dc}^*. The error is sent to the voltage regulator $\mathrm{G_{VDC}}$, implemented by a proportional-integral compensator, whose output then sets the reference for active component magnitude of the output voltage, i.e., v_{Cpm}^* The average dc voltage is determined by the total active power absorbed by the injector, which can be regulated with active component magnitude of the output voltage v_{Cp}, and thus the average dc voltage controller works.

It is supposed that the system current is expressed by (1), where f_0 denotes the fundamental frequency of the ac system. Then its phase angle θ is extracted by the PLL, which can be implemented by conventional second order generalized integrator based PLL for single-phase system [16]. Giving the reference for the active component magnitude of the output voltage v_{Cpm}^* and phase angle of system current θ, the instantaneous output voltage reference v_C^* is synthesized, which is shown in Fig. 3(b). Then the error between the reference of the output voltage and the actual output voltage is sent to the ac voltage regulator $\mathrm{G_{VC}}$, which generate a common reference for the inductor current of each H-bridge converter i_L^*. Since the actual output voltage will track its instantaneous reference by regulating the inductor currents, the perturbation reference v_P^* is added as a part of the instantaneous output voltage reference to achieve the second control target.

$$i_{Sa} = I_{Sm}\sin\left(2\pi f_0 t + \theta_0\right) = I_{Sm}\sin\theta. \tag{1}$$

The third target is realized by the dc voltage balancing control, whose inner structure is shown in Fig. 3(c). DC voltage of each H-bridge converter v_{dck} is compared with the average value of all dc voltages $\overline{v_{dc}}$, and the error is sent to the trimming regulator $\mathrm{G_{ILt}}$. It generates the magnitude reference of the trimming component for the inductor current in corresponding H-bridge converter, which is further multiplied by the sinusoidal value of

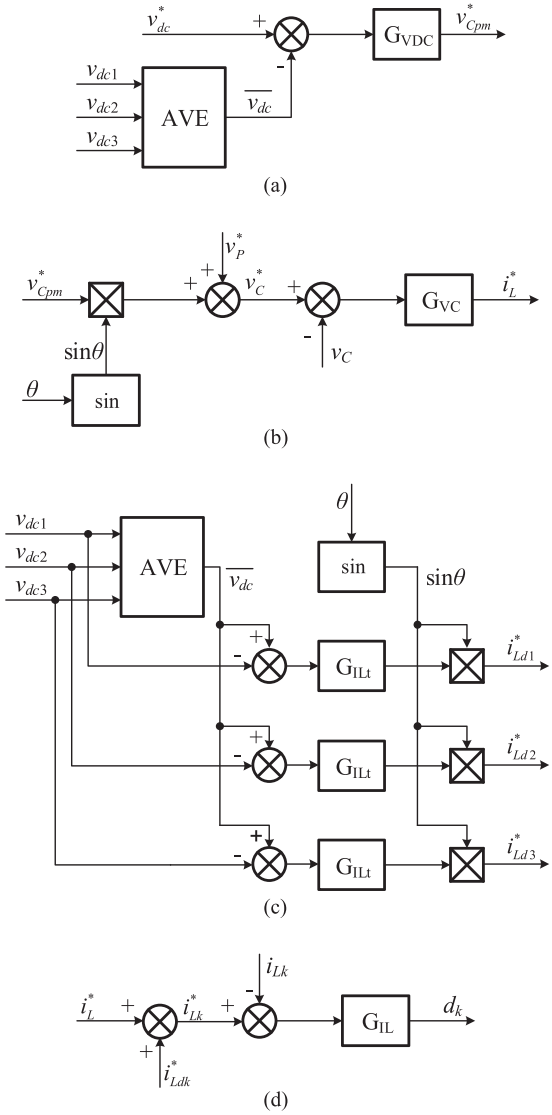

Fig. 3. Inner structure of (a) average dc voltage control, (b) ac voltage control, (c) dc voltage balancing control, and (d) ac current control in existing control scheme.

the phase angle θ to produce the instantaneous reference i_{Ldk}^* of the trimming component. As shown in Fig. 3(d), the inductor current reference for each H-bridge converter eventually consists of the common component i_L^* and the trimming component i_{Ldk}^*, while it is able to redistribute the active power flowing into H-bridge converters sharing common output voltage v_C by trimming their inductor currents, and thus the dc voltages could be balanced by slightly adjusting the inductor current references through their trimming components. It is worth mentioning that as expressed in (2) the sum of all trimming component references equals to zero and the total active power absorbed by the series injector is not impacted by the dc voltage balancing control

$$\sum_{k=1}^{N} i_{Ldk}^* = 0. \tag{2}$$

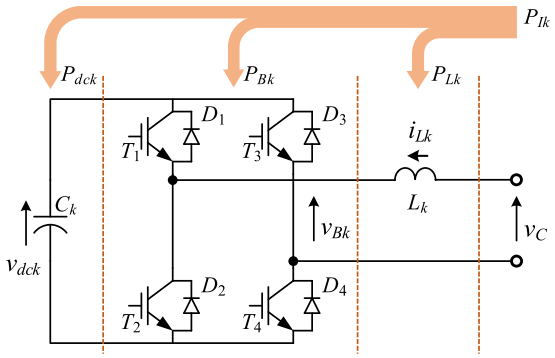

Fig. 4. Active power flow of an H-bridge converter with float dc capacitor.

Besides, it is obvious that fourth target, i.e., the system current sharing among the H-bridge converters, can be met by the ac current control for each H-bridge converter shown in Fig. 3(d). Each inductor current i_{Lk} is controlled to track its reference i^*_{Lk} by regulating the duty cycle of the H-bridge converter with the ac current compensator $G_{\rm IL}$.

B. Active Power Modeling of H-Bridge Converter

In the H-bridge converter, the dc voltage v_{dck} is relative to the active power absorbed at its ac terminal as well as the power eventually flowing into the dc capacitor C_k. Thus, it is necessary to model the active power flow of each H-bridge converter for analyzing the mechanism behind the dc voltage imbalance of PHB-based series injector.

As shown in Fig. 4, the average active power absorbed at its terminal P_{Ik} will equal to the sum of the power losses of the inductor P_{Lk}, the power losses of the H-bridge P_{Bk} and the power flowing into dc side P_{dck}, and their relationship is presented in (3). To facilitate generalizing the power losses analysis, the inductor current is expressed in (4)

$$P_{Ik} = P_{Lk} + P_{Bk} + P_{dck} \tag{3}$$

$$i_{Lk} = I_{Lkm} \sin \varphi. \tag{4}$$

The inductor power losses P_{Lk} consist of copper loss and core loss. The copper loss, introduced by the resistance of the winding, is expressed in (5) [17]. As shown in (6), the core loss is determined the frequency, the magnitude of the magnetic density, and the characteristic of core material [18]. The parameter β is determined by the core material, and generally close to 2. Therefore, the total power losses of inductor can be expressed in (7), and its equivalent resistance R_{Lk} is less dependent of the inductor current and given by (8) approximately, where k_i denotes the ratio from the magnetic density to the inductor current

$$P_{copper} = \frac{1}{2} I^2_{Lkm} R_{wind} \tag{5}$$

$$P_{core} = K_c f^{\alpha} B^{\beta}_m \tag{6}$$

$$P_{Lk} = \frac{1}{2} I^2_{Lkm} R_{Lk} \tag{7}$$

$$R_{Lk} \approx R_{wind} + \frac{K_c f^{\alpha} k_i^2}{2}. \tag{8}$$

To estimate the losses of H-bridge, the loss models of the power semiconductor devices are listed below [19], [20]. For the IGBT, the ON-state voltage drop is presented in (9), and turn ON loss and turn OFF loss are given in (10) and (11), respectively. For the diode, the ON-state voltage drop is presented in (12), and during the transient, only the power loss caused by reverse recovery is considered, which is expressed in (13). All parameters in these models can be extracted from the device datasheet

$$v_{on} = V_t + R_{ce} i_c \tag{9}$$

$$E_{on} = A_{on} i_c \frac{v_{ce}}{V_{base}} \tag{10}$$

$$E_{off} = A_{off} i_c \frac{v_{ce}}{V_{base}} \tag{11}$$

$$v_{on} = V_f + R_{ak} i_d \tag{12}$$

$$E_{rec} = A_{rec} i_d \frac{v_{ak}}{V_{base}}. \tag{13}$$

The bipolar strategy is adopted for pulsewidth modulation in H-bridge, and all the power semiconductor switches are symmetrical. In each switch, it is reasonable to suppose that the IGBT and the diode, being with the same current rating and voltage rating, share the same conduction characteristics. Therefore, the total power losses of the H-bridge can be derived and simplified to the following equation:

$$P_{Bk} = M_{Bk1} I_{Lkm} + M_{Bk2} I^2_{Lkm} \tag{14}$$

where

$$M_{Bk1} = \frac{4}{\pi} \left[V_f + \frac{v_{dck}}{V_{base}} f_s \left(A_{on} + A_{off} + A_{rec} \right) \right]$$

$$M_{Bk2} = R_{ce} = R_{ak}.$$

The deduction process for (14) will be presented in Appendix, and it is obvious that the power losses of the H-bridge consist of two terms. The first term, where f_s denotes the switching frequency, is determined by the switching behaviors and the constant components of the ON-state voltage drops. The second term is introduced by the slopes of the ON-state voltage drop variation with the conduction current.

Finally, the active power flowing into the dc capacitor is used to compensate its power loss that generally increases with its terminal dc voltage, and the dc voltage will increase until its power loss just equals to the active power flowing into dc capacitors.

C. Analysis of DC Voltage Imbalance in Existing Control Scheme

In existing control scheme, it could be supposed that the steady-state errors of the ac current control and the ac voltage control around fundamental frequency are zero because their

bandwidths are much higher than the fundamental frequency. Besides, the perturbation frequency component of the output voltage can be neglected since it has less influence on the active power flow in steady state. Therefore, the output voltage can be expressed in (15), where V_{Cpm} is equal to the reference generated by the average dc voltage control

$$v_C = V_{Cpm}\sin\theta. \tag{15}$$

Then the inductor current of each H-bridge converter consists of the common component and the trimming component. As mentioned above, the sum of all trimming components is zero and the common components are identical to each other. Therefore, the common component of the inductor current will almost be in phase with the system current i_{Sa} with the assumption that the current of ac capacitor is negligible since its capacitance C_p is very small, and it can be presented in (16). Furthermore, the trimming component of the inductor current is also in phase with the system current in the existing control scheme according to Fig. 3(c). Eventually, the inductor current can be presented in (17), whose magnitude I_{Lkpm} is associated with the system current magnitude and the trimming component magnitude I_{Ldkm} in (18)

$$i_L = \frac{1}{N}i_{Sa} = \frac{I_{Sm}}{N}\sin\theta \tag{16}$$

$$i_{Lk} = I_{Lkpm}\sin\theta \tag{17}$$

$$I_{Lkpm} = \frac{I_{Sm}}{N} + I_{Ldkm}. \tag{18}$$

Combining (15) and (17), the absorbed active power of the H-bridge converter can be derived, which is presented in the following equation:

$$P_{Ik} = \frac{1}{2\pi}\int_0^{2\pi} v_C i_{Lk}\,d\theta = \frac{1}{2}V_{Cpm}I_{Lkpm}. \tag{19}$$

Then substitute (18) into (7) and (14), the inductor power losses and the bridge power losses are obtained for the existing control scheme. Furthermore, the output voltage magnitude can be derived by combing (3) and (19), which is presented in (20). It is found that the output voltage magnitude will decrease and then increase with the inductor current magnitude

$$V_{Cpm} = 2M_{Bk1} + R_{Lk}I_{Lkpm} + 2M_{Bk2}I_{Lkpm} + \frac{2P_{dck}}{I_{Lkpm}}. \tag{20}$$

According to (18), the inductor current magnitude is actually trimmed to balance the dc voltages, while the dc voltage is determined the active power flowing into dc capacitors P_{dck} in each H-bridge converter. Therefore, it is significant to get the mathematical relationship between the dc power and the inductor current magnitude, which can be derived by substituting (7), (14) and (19) into (3), and finally be presented in the following equation:

$$P_{dck} = \frac{1}{2}V_{Cpm}I_{Lkpm} - M_{Bk1}I_{Lkpm} - \left(M_{Bk2} + \frac{1}{2}R_{Lk}\right)I_{Lkpm}^2. \tag{21}$$

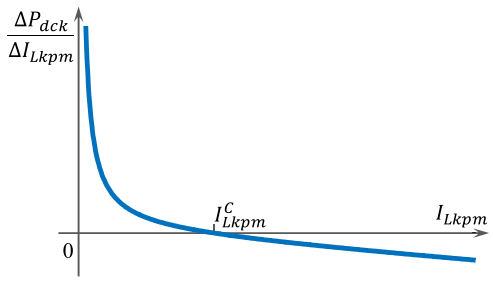

Fig. 5. Impact of inductor current magnitude on the derivative of the dc power with respect to the inductor current magnitude in the H-Bridge converter with the existing control scheme.

Since the inductor current magnitude is trimmed in the dc voltage balancing control of existing scheme, it is necessary to investigate the impact of the inductor current magnitude variation on the dc power variation, which can be mathematically represented by the derivative of the dc power with respect to the inductor current magnitude. This derivative can be obtained from (21) by combining (20), which is shown in (22). It is obvious that the value of the derivation is determined by the operation points of the inductor current magnitude as well as the dc power

$$\frac{\Delta P_{dck}}{\Delta I_{Lkpm}} = \frac{P_{dck}}{I_{Lkpm}} - \left(\frac{R_{Lk}}{2} + M_{Bk2}\right)I_{Lkpm}. \tag{22}$$

As shown in Fig. 5, the derivative of the dc power with respect to the inductor current magnitude will be positive when the inductor current magnitude is less than a critical point and be negative when it is larger than the critical point which is given in (23). It can be found that the critical point is just determined by parameters of the inductor and the power semiconductor devices as well as the power flowing into the dc capacitor in the H-bridge converter. Besides, at the critical point, the power flowing into dc capacitor exactly equal to the so-called resistive losses in this paper, which consist of inductor losses and the second term of the H-bridge losses and are proportional to the square of inductor current magnitude

$$I_{Lkpm}^C = \sqrt{\frac{P_{dck}}{\frac{R_{Lk}}{2} + M_{Bk2}}}. \tag{23}$$

This derivative expressed in (22) means that when the inductor current magnitude is lower than the critical point I_{Lkpm}^C, power flowing into dc capacitor P_{dck} will increase with inductor current magnitude I_{Lkpm}, and the dc voltage balancing control works well. When the inductor current magnitude exceeds the critical point, power flowing into dc capacitor P_{dck} will decrease with inductor current magnitude I_{Lkpm}, and thus a positive feedback appears in the dc voltage balancing loop. Consequently, in existing control scheme, the dc voltages cannot be balanced anymore when the inductor current magnitude is larger than the critical point.

According to (18), the inductor current magnitude will increase with system current magnitude, and there must be a critical point for the system current magnitude I_{Sm}^C, which can be expressed in (24) since the trimming component is much less

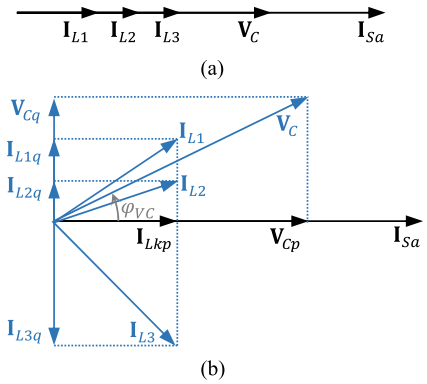

Fig. 6. Phasor diagram of inductor currents and output voltage in PHB-based series injector with (a) existing scheme, and (b) proposed scheme. In the proposed scheme, output voltage v_C consists of active component v_{Cp} and reactive component v_{Cq}, while inductor current i_{Lk} consists of active component i_{Lkp} and reactive component i_{Lkq}.

than the common component in the inductor current. Therefore, the dc voltages will be imbalance when the system current magnitude is larger than its critical point

$$I_{Sm}^{C} \approx N \cdot \sqrt{\frac{P_{dck}}{\frac{R_{Lk}}{2} + M_{Bk2}}}. \tag{24}$$

Moreover, in the steady state, the power flowing into dc capacitor P_{dck}, which is equal to the power loss of the dc capacitor C_k in steady state, generally is much less than the resistive losses in the H-bridge converter, and therefore the critical point of the inductor current magnitude shown in (23) will be much less than the inductor current rating. Consequently, the operation range of the series injector with existing control scheme is seriously restricted.

IV. Enhanced Control Scheme

To tackle the aforementioned issue in existing control scheme, this paper proposes an enhanced control scheme to balance the dc voltages in the full system current range for PHB-based series injector.

A. Basic Principle

As mentioned above, in the existing scheme, the inductor currents are in phase with the system current and inductor current magnitudes are trimmed to redistribute the active powers among H-bridge converters for balancing their dc voltages, and their phasors can be presented in Fig. 6(a). Thus the dc voltage balancing control is tightly coupled with the system current magnitude, and the derivative of the dc power with respect to the inductor current magnitude will be negative when the system current magnitude exceeds the critical point.

In order to decouple the dc voltage balancing control from the system current magnitude, reactive circulating currents are introduced among H-bridge converters for balancing their dc voltages in the proposed scheme, where the phasors of inductor currents and output voltage are presented in Fig. 6(b). The inductor current of each H-bridge converter consists of the active component i_{Lkp} and the reactive component i_{Lkq}. The active components of the inductor currents are in phase with the system current and share identical magnitude. The reactive components of the inductor currents lag or lead the system current by 90°, and their sum is zero according to Kirchhoff's current law. Furthermore, a reactive component v_{Cq} is injected into the output voltage for achieving redistribution of active power among H-bridge converters.

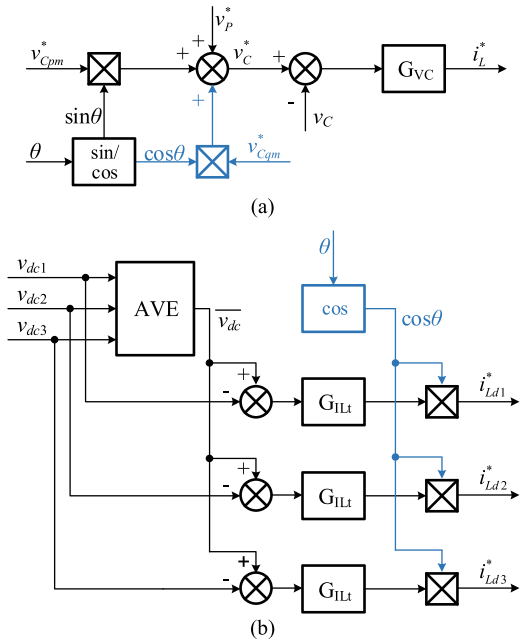

Fig. 7. Inner structures of (a) ac voltage control and (b) dc voltage balancing control in the proposed scheme.

Therefore, the interaction between the active component of inductor current and the active component of output voltage will product identical active power in each H-bridge converter. Meanwhile, the interaction between the reactive components of inductor currents and the reactive component of output voltage will also generate active powers, and thus the active power absorbed by H-bridge converters will be slightly redistributed. Consequently, the amount of redistribution active power can be regulated by trimming the reactive components of inductor currents i_{Lkq}.

B. Control Block Diagram

Based on the basic principle of the enhanced control scheme, the ac voltage control and the dc voltage balancing control in existing scheme should be improved, and their block diagrams in the proposed control scheme are presented in Fig. 7.

Compared to existing ac voltage control shown in Fig. 3(b), the instantaneous output voltage reference v_C^* of the proposed scheme is enhanced by adding an additional part, i.e., the reactive component, whose magnitude v_{Cqm}^* is fixed and will be designed in the following part of this paper.

In the PHB-based series injector, the dc voltage balancing control is realized by trimming the inductor currents of each H-bridge converter. In the existing dc voltage balancing control

scheme, the inductor current of each H-bridge converter is always in phase with the output voltage, and their inductor current magnitudes are trimmed based on their dc voltage. In the proposed dc voltage balancing control, the output of each trimming regulator G_{ILt} is multiplied by the cosine value of the phase angle θ, and thus the generated trimming component references i^*_{Ldk} are orthogonal to the system current.

C. Performance Analysis

Since the frequency of introduced reactive component in the output voltage reference is much lower than the bandwidth of ac voltage loop, the instantaneous output voltage can be expressed in (25), where V_{Cqm} is equal to reactive component magnitude reference v^*_{Cqm}. It is worth noting that the overall active power absorbed by the whole series injector is not changed by this reactive component of the output voltage, and the original overall dc voltage loop is not impacted

$$v_C = V_{Cpm}\sin\theta + V_{Cqm}\cos\theta. \tag{25}$$

Then the inductor current of each H-bridge converter, consisting of the common component and the trimming component, can be presented in (26). Similar to the existing control scheme, the common component of the inductor current in the proposed control scheme is in phase with the system current, and its magnitude is expressed in (27). Besides, the inductor current magnitude is expressed in (28)

$$i_{Lk} = i^*_L\sin\theta + i^*_{Ldk} = I_{Lkpm}\sin\theta + I_{Lkqm}\cos\theta \tag{26}$$

$$I_{Lkpm} = \frac{I_{Sm}}{N} \tag{27}$$

$$I_{Lkm} = \sqrt{I^2_{Lkpm} + I^2_{Lkqm}}. \tag{28}$$

Combining (25) and (26), the absorbed active power of each H-bridge converter can be derived and presented in (29). It can be found that the active power is composed by two parts, and the first part is introduced by the active component of the output voltage and the common part of the inductor current, which is identical to each other. The second part is caused by the interaction between the reactive component of the output voltage and the trimming part of the inductor current, and it is obvious that the sum of these second parts among all H-bridge converters will be zero. Therefore, the active power can be redistributed among H-bridge converters by trimming the reactive components of inductor currents

$$P_{Ik} = \frac{1}{2\pi}\int_0^{2\pi} v_C i_{Lk} d\theta = \frac{1}{2}V_{Cpm}I_{Lkpm} + \frac{1}{2}V_{Cqm}I_{Lkqm}. \tag{29}$$

Then power losses of the inductor and H-bridge in the proposed scheme can be obtained by substituting (28) into (7) and (17) separately. Furthermore, the active power flowing into dc capacitors in each H-bridge converter can be derived by combing (29) and (3), which is presented in (30).

$$\begin{aligned} P_{dck} = {} & \frac{1}{2}V_{Cpm}I_{Lkpm} + \frac{1}{2}V_{Cqm}I_{Lkqm} \\ & - \frac{1}{2}R_{Lk}\left(I^2_{Lkpm} + I^2_{Lkqm}\right) \\ & - M_{Bk1}\sqrt{I^2_{Lkpm} + I^2_{Lkqm}} \\ & - M_{Bk2}\left(I^2_{Lkpm} + I^2_{Lkqm}\right). \end{aligned} \tag{30}$$

Since the reactive component magnitude of the inductor current is trimmed in dc voltage balancing control of proposed scheme, it is necessary to investigate the impact of its reactive component magnitude variation on the dc power variation, which can be mathematically represented by the derivative of the dc power with respect to the reactive component magnitude of the inductor current. This derivative can be obtained from (30), which is presented in (31). Since the reactive component of the inductor current is just used to slightly redistribute the active power among H-bridge converters, which is much less than the active component of the inductor current, (31) can be simplified as (32)

$$\begin{aligned} \frac{\Delta P_{dck}}{\Delta I_{Lkqm}} = {} & \frac{1}{2}V_{Cqm} - \left(R_{Lk} + 2M_{Bk2}\right)I_{Lkqm} \\ & - \frac{M_{Bk1}I_{Lkqm}}{\sqrt{I^2_{Lkpm} + I^2_{Lkqm}}} \end{aligned} \tag{31}$$

$$\frac{\Delta P_{dck}}{\Delta I_{Lkqm}} \approx \frac{1}{2}V_{Cqm} - \left(R_{Lk} + 2M_{Bk2} + \frac{M_{Bk1}}{I_{Lkpm}}\right)I_{Lkqm}. \tag{32}$$

In (32), it is obvious that the derivative is mainly dependent of two factors, i.e., the reactive component magnitude of the output voltage and the reactive component magnitude of the inductor current, and it will increase with the first factor while decrease with the second factor. In existing scheme, the derivative shown in (22), associated with dc voltage balancing, is just determined by system current magnitude and will be negative when the system current is larger than the critical point presented in (23). However, in the proposed scheme, the corresponding derivative, presented in (32), can be kept positive if the reactive component magnitude of the output voltage is large enough. Consequently, the dc voltage balancing control in the proposed scheme is always negative feedback, and dc voltages can be balanced with less impact from the system current magnitude.

Besides, in the proposed scheme, the output voltage is no more in phase with the system current, and its phase angle referring the system current can be expressed in (33), which is determined by the reactive component magnitude and active component magnitude of the output voltage

$$\varphi_{VC} = \tan^{-1}\frac{V_{Cqm}}{V_{Cpm}}. \tag{33}$$

Similar to the existing scheme, the active component magnitude V_{Cpm} is regulated by the overall dc voltage control shown in Fig. 3(a), and it will decrease and then increase with

the increase of system current magnitude according to (20). Meanwhile, the reactive component magnitude of the output voltage is fixed. Therefore, with the increase of system current magnitude, the phase angle of output voltage φ_{VC} will increase and then decrease.

During impedance measurement, the perturbation voltage with the magnitude of V_{pm} is injected, and the output voltage of series injector can be expressed as follows:

$$v_C = V_{Cpm}\sin(2\pi f_0 t + \theta_0) + V_{Cqm}\cos(2\pi f_0 t + \theta_0) + V_{pm}\sin(2\pi f_p t + \varphi_p) \tag{34}$$

where f_p is the perturbation frequency. It is obvious that being the same as the active component, the reactive component injected into the output voltage is always frequency independent of the perturbation component, and thus the impedance measured at f_p will be less impacted by the reactive component of the output voltage.

V. Parameter Design

In the proposed scheme, the reactive component magnitude of output voltage must be large enough to make the derivative of the dc power with respect to the reactive component magnitude of inductor current be positive. However, if this reactive component magnitude is extremely large, extra voltage stress on the devices of the H-bridge converter will happen and the operation point of the load will be seriously influenced. Therefore, the reference of reactive component magnitude v^*_{Cqm} in output voltage should be designed properly.

A. Modeling of H-Bridge Converter Variance

As mentioned above, the absorbed active power of each H-bridge converter shown in (29) consists of two parts. The first part of each converter is identical to the one of each other, while the second part is used to compensate power loss differences among converters caused by the converter variances. Therefore, the average value of absorbed active power among all converters can be presented in the following equation:

$$\overline{P_I} = \overline{P_{dc}} + \frac{\overline{R_L}}{2}I^2_{Lkpm} + \overline{M_{B1}}I_{Lkpm} + \overline{M_{B2}}I^2_{Lkpm} = \frac{1}{2}V_{Cpm}I_{Lkpm} \tag{35}$$

where

$$\overline{P_{dc}} = \frac{1}{N}\sum_{k=1}^{N}P_{dck}$$

$$\overline{R_L} = \frac{1}{N}\sum_{k=1}^{N}R_{Lk}$$

$$\overline{M_{B1}} = \frac{1}{N}\sum_{k=1}^{N}M_{Bk1}$$

$$\overline{M_{B2}} = \frac{1}{N}\sum_{k=1}^{N}M_{Bk2}.$$

Defining the overall variance factor for the kth H-bridge converter as γ_k, its active power absorbed can be expressed in the following equation:

$$P_{Ik} = (1+\gamma_k)\,\overline{P_I}. \tag{36}$$

It is obvious that the overall variance factor is a weighted average on the variance factors of devices, and the relationship among them can be presented in the following equation:

$$\gamma_k = \frac{\overline{P_{dc}}}{\overline{P_I}}\cdot\gamma_{dck} + \frac{\frac{\overline{R_L}}{2}I^2_{Lkpm}}{\overline{P_I}}\cdot\gamma_{Lk} + \frac{\overline{M_{B1}}I_{Lkpm}}{\overline{P_I}}\cdot\gamma_{Bk1} + \frac{\overline{M_{B2}}I^2_{Lkpm}}{\overline{P_I}}\cdot\gamma_{Bk2} \tag{37}$$

where

$$\gamma_{dck} = \frac{P_{dck}}{\overline{P_{dc}}} - 1$$

$$\gamma_{Lk} = \frac{R_{Lk}}{\overline{R_L}} - 1$$

$$\gamma_{Bk1} = \frac{M_{Bk1}}{\overline{M_{B1}}} - 1$$

$$\gamma_{Bk2} = \frac{M_{Bk2}}{\overline{M_{B2}}} - 1.$$

Therefore, as shown in (37), the overall variance factor γ_k must be between the minimum value and the maximum value among variance factors of devices. The variance factors of devices can be calculated based on their parameter tolerances, and thus it is convenient to estimate the overall variance factor γ_k in the following equation:

$$\min\{\gamma_{dck},\gamma_{Lk},\gamma_{Bk1},\gamma_{Bk2}\} \le \gamma_k \le \max\{\gamma_{dck},\gamma_{Lk},\gamma_{Bk1},\gamma_{Bk2}\}. \tag{38}$$

B. Design Criterion

It is supposed the converter variance factor is given, and then the operation points of reactive component magnitude in both output voltage and inductor current with given system current can be obtained by combining (26) and (35), which is presented in (39). Therefore, the reactive component magnitude of output voltage decreases with the reactive component magnitude of the inductor current, and the operation trace is presented in Fig. 8. With the increase of system current, i.e., the active component magnitude of inductor current I_{Lkpm}, the trace will move up since the average active power absorbed by the H-bridge converter raises

$$V_{Cqm} = \frac{2\gamma_k\overline{P_I}}{I_{Lkqm}}. \tag{39}$$

Even though the power loss difference caused by the converter variance can be compensated by the active power introduced by the reactive components of the output voltage and inductor current, which are presented by each point on the operation trace, the dc voltage balance is not guaranteed. Then the dc voltage balancing boundary under different system current is presented in Fig. 8 by setting the derivation shown in (32) to zero. It can be found that there is an intersection between the original operating trace and the dc voltage balancing boundary, and thus

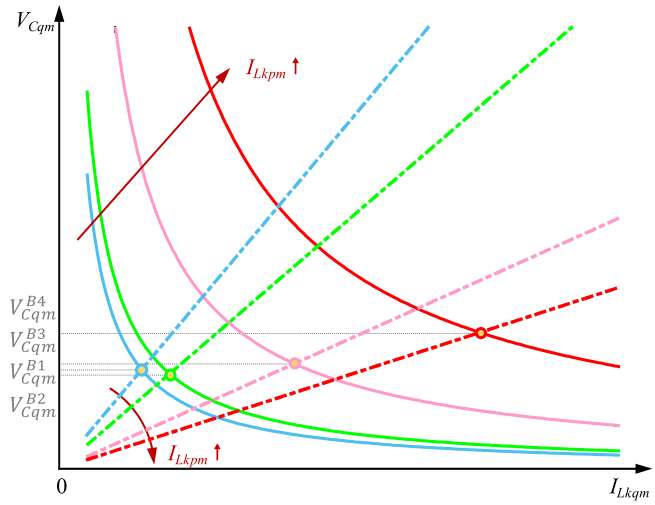

Fig. 8. Boundary deduction for the reactive component magnitude of the output voltage, where solid lines and dot dash lines present the operation trace and the dc voltage balancing boundary separately under four cases with the different active component magnitude of the inductor current. The intersection between the operation trace and the dc voltage balancing boundary sets the boundary for the reactive component magnitude of the output voltage.

the operation trace is divided into two parts, i.e., left part and right part. It is obvious that the points at the left part of the operation trace will make the derivative of the dc power with respect to the reactive component magnitude of inductor current be positive and the dc voltages are balanced. Therefore, to keep the dc voltages balance, the operation point of the reactive component magnitude of output voltage must be larger than its boundary presented by the intersection point in Fig. 8. Besides, the boundary of the reactive component magnitude of the output voltage can be calculated out by combining (32) and (39), which is expressed in the following equation:

$$V_{Cqm}^{B} = 2\sqrt{\gamma_k} \cdot \sqrt{(R_{Lk} + 2M_{Bk2}) \cdot \overline{P_I} + M_{Bk1} \cdot \frac{\overline{P_I}}{I_{Lkpm}}}. \tag{40}$$

In Fig. 8, it can also be observed that the location of the intersection moves with the active component magnitude of inductor current I_{Lkpm}, and thus the boundary of the reactive component magnitude of output voltage V_{Cqm}^{B} is varied. According to (35), the average active power $\overline{P_I}$ increases rapidly with the active component magnitude of the inductor current. Therefore, as shown in Fig. 9, the boundary of the reactive component magnitude of output voltage V_{Cqm}^{B} will decrease and then increase with the active component magnitude of the inductor current. It reaches the peak value $V_{Cqm}^{B(\max)}$ under the condition of maximum active component magnitude of inductor current $I_{Lkpm(\max)}$, i.e., the condition of the maximum system current.

Eventually, in order to guarantee the derivative shown in (32) be positive under full system current range, the reference of the reactive component magnitude of output voltage v_{Cqm}^{*} must always be larger than the boundary shown in (40). And this requirement can be met if it is larger than the boundary $V_{Cqm}^{B(\max)}$ under maximum system current. Therefore, v_{Cqm}^{*} can be designed in (41), where the maximum average active power $\overline{P_{I(\max)}}$ can be calculated out by substituting the maximum

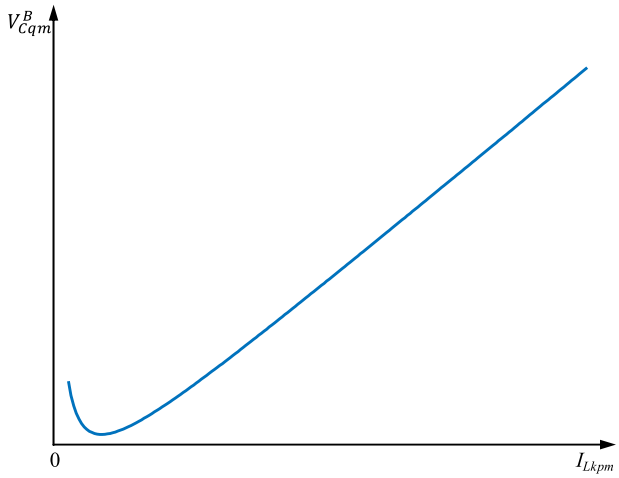

Fig. 9. Variation of the reactive component magnitude boundary of output voltage V_{Cqm}^{B} with the active component magnitude of inductor current I_{Lkpm}.

active component magnitude of inductor current $I_{Lkpm(\max)}$ into (35)

$$v_{Cqm}^{*} > 2\sqrt{\gamma_k} \cdot \sqrt{(R_{Lk} + 2M_{Bk2}) \cdot \overline{P_{I(\max)}} + M_{Bk1} \cdot \frac{\overline{P_{I(\max)}}}{I_{Lkpm(\max)}}} \tag{41}$$

In summary, to keep dc voltages balance under full system current range, the reference of the reactive component magnitude of the output voltage v_{Cqm}^{*} in the proposed control scheme can be designed according to the overall converter variance factor, the parameters of devices and the maximum system current magnitude.

VI. Simulation and Experimental Results

To verify the imbalance mechanism of dc voltages in the existing scheme and investigate the feasibility of the proposed scheme, both simulation and experiment have been performed.

A. Simulation Results

A PHB-based series injector composed of three H-bridge converters is a simulation in SABER. The system configuration can be presented in Fig. 1, while the output terminal of the series injector is connected to a current sink denoting the system current. In the simulation, the voltage drop and switching transient of power semiconductor devices are neglected for simplification, and the power losses of H-bridge converter are just introduced by the ESR of ac inductor R_{Lk} and the equivalent parallel resistance (EPR) of dc capacitor R_{dck}. Parameters of PHB in the simulation are listed in Table I. Moreover, variance factors of R_{Lk} and R_{dck} are set to 3%, 0, and −3%, respectively.

Substituting corresponding parameters in Table I into (24), the critical point of system current magnitude I_{Sm}^{C} can be calculated out, which is 17.4 A. It means that the dc voltages will be imbalance when the system current magnitude is larger than 17.4 A. Then the PHB-based series injector with an existing scheme is simulated under different system current magnitudes, and the simulation results are shown in Fig. 10. In Fig. 10(a), the

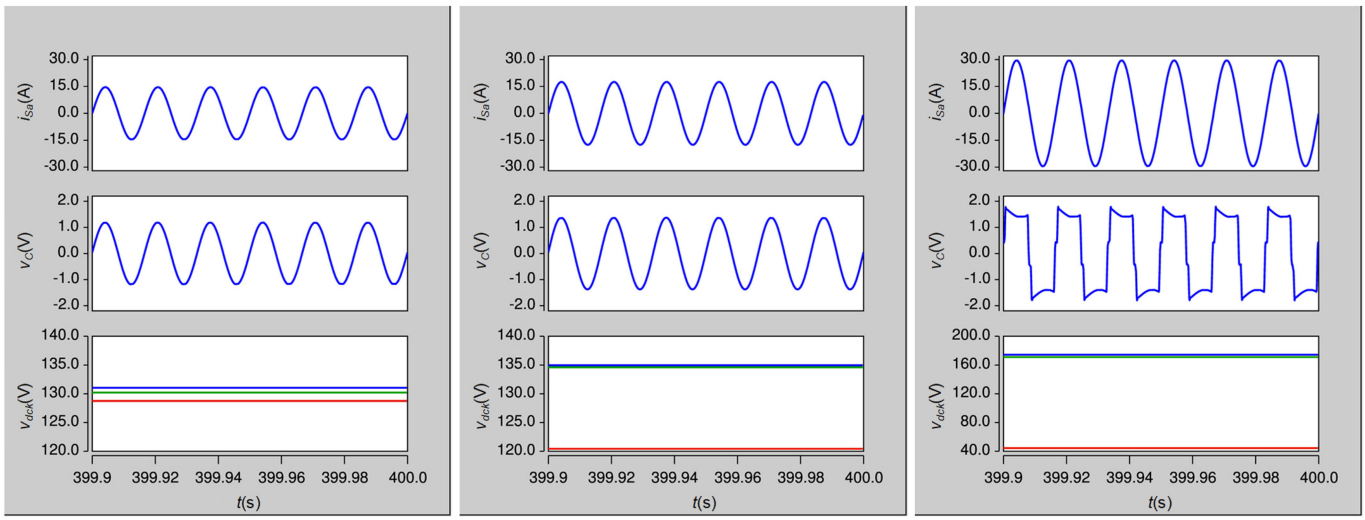

Fig. 10. Simulation waveforms of system current i_{Sa}, output voltage v_C and dc capacitor voltages v_{dck} in PHB with the existing scheme under (a) $I_{Sm} = 15$ A, (b) $I_{Sm} = 18$ A, and (c) $I_{Sm} = 30$ A.

TABLE I
PARAMETERS OF PHB-BASED SERIES INJECTOR IN THE SIMULATION

Symbol	Description	Value
C_k	DC capacitor	16.4 mF
L_k	AC inductor	0.66 mH
$\overline{R_{dc}}$	Average EPR of DC capacitor	10 kΩ
$\overline{R_L}$	Average ESR of AC inductor	100 mΩ
C_p	AC capacitor	66 μF
v_{dc}^*	DC voltage reference	130 V
v_{pm}^*	Perturbation reference magnitude	0 V

system current magnitude is lower than its critical point, and dc voltages should be balanced. It can be seen from the waveforms of v_{dck} that dc voltages are almost balanced, and their tiny steady state errors are caused by the proportional compensator used in the trimming regulator $\mathrm{G_{ILt}}$. In Fig. 10(b), the system current magnitude is larger than its critical point, and dc voltages will be imbalance. It can be observed that the maximum dc voltage error is 10 V, and the dc voltage is not balanced obviously. Finally, the system current magnitude is increased to 30 A, and it can be found in Fig. 10(c) that the maximum dc voltage error is enlarged to 90 V and serious distortion appears in the waveform of the output voltage.

To further verify the accuracy of the critical point I_{Sm}^C, the average EPR of dc capacitors is changed to 8 kΩ, and the critical point I_{Sm}^C is increased to 19.5 A. Then the PHB-based series injector with an existing scheme is simulated again and the simulation results are presented in Fig. 11. In Fig. 11(b), the system current magnitude is lower than its critical point, and dc voltages should be balanced. It can be seen from the waveforms of dc voltages v_{dck} that the error is less than 2 V, and dc voltages are almost balanced. In Fig. 11(c), the system current magnitude is still larger than its critical point, and dc voltages will be imbalanced. This is demonstrated by waveforms of dc voltages with maximum dc voltage error of 60 V. Consequently, the imbalance mechanism analysis of dc voltages as well as the derived critical point of system current magnitude in PHB with the existing scheme are verified. At last, the PHB with the proposed scheme is simulated using the parameters listed in Table I. In Fig. 12(a), the system current magnitude is set to 18 A, which is identical to the one used in Fig. 10(b). However, there are two major differences between the waveforms of Fig. 12(a) and Fig. 10(b). First, the output voltage leads the system current in Fig. 12(a) since the injected reactive component in output voltage; second, the maximum dc voltage error in Fig. 12(a) is around 2 V, which is much less than the one in Fig. 10(b). Therefore, under the system current magnitude of 18 A, dc voltages in the PHB with the existing scheme are imbalance while they are balanced with the proposed scheme, and the feasible of the proposed scheme is demonstrated. Then the system current magnitude is increased to 30 A, and dc voltages are still balanced even though the maximum dc voltage error increases a little bit. This phenomenon is caused by the proportional compensator used for trimming regulator $\mathrm{G_{ILt}}$, and this dc voltage error can be mitigated by reducing the output of the trimming regulator through increasing the reactive component magnitude of the output voltage. Thus, the reference of the reactive component magnitude of the output voltage is increased to 0.5 V, and the maximum dc voltage error is reduced in Fig. 12(c).

B. Experimental Results

An experimental prototype of ac impedance measurement setup consisting of a PHB-based series injector has been built up which is shown in Fig. 13, where three H-bridge converters are covered. In each H-bridge converter, the power semiconductor switches are implemented by an intelligent power module PM75CL1A120 from POWEREX. Besides, the injector controller is implemented fully digitally by an MCU TMS320C28343 from Texas Instruments. The configuration of the overall experimental test system is shown in Fig. 14, where the source subsystem and the load subsystem are implemented by a programmable ac source and a resistor bank separately.

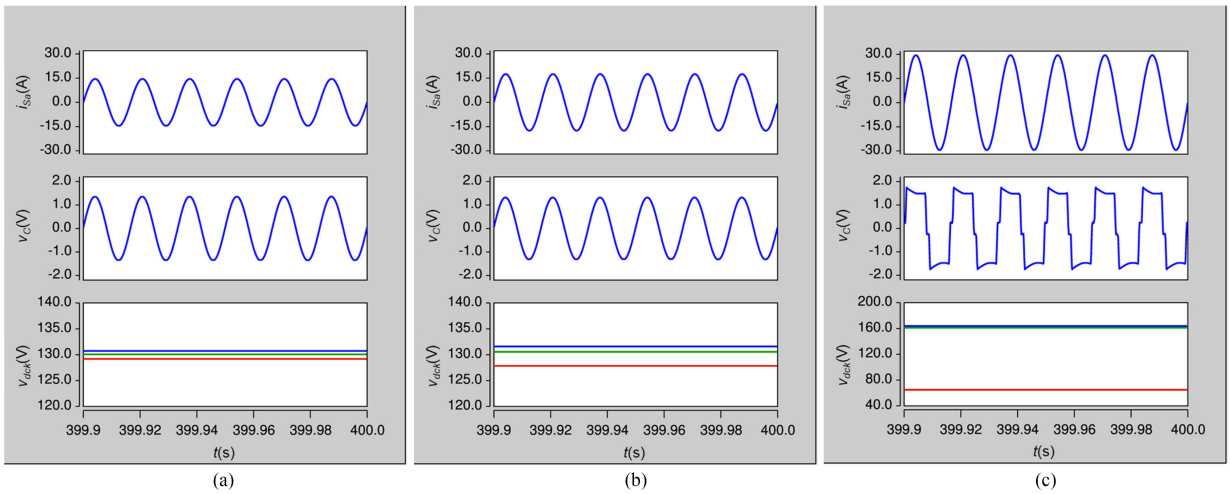

Fig. 11. Simulation waveforms of system current i_{Sa}, output voltage v_C and dc capacitor voltages v_{dck} in PHB with the existing scheme under (a) $I_{Sm} = 15$ A, (b) $I_{Sm} = 18$ A, and (c) $I_{Sm} = 30$ A when the average EPR of dc capacitors is changed to 8 kΩ.

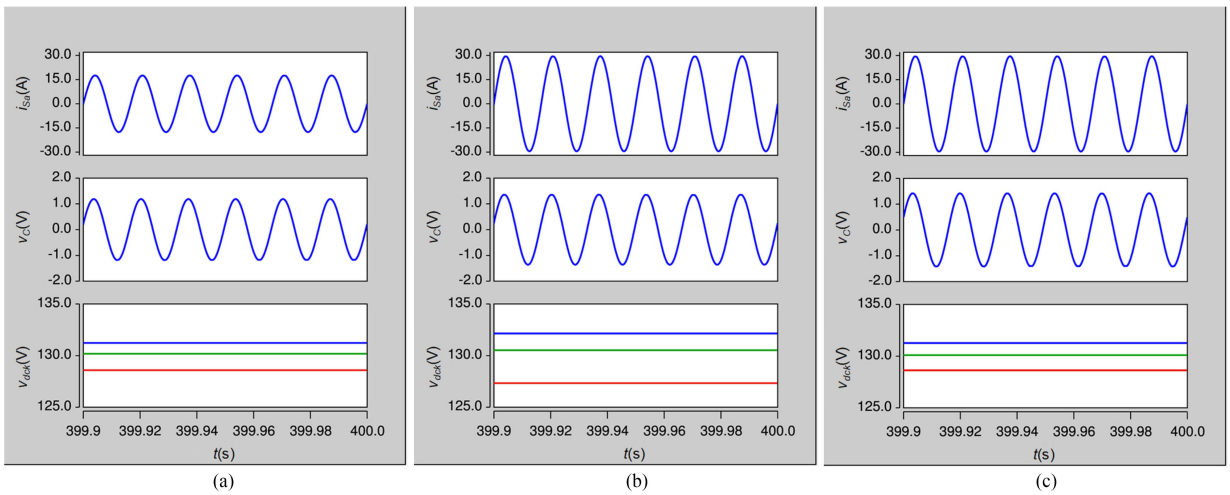

Fig. 12. Simulation waveforms of system current i_{Sa}, output voltage v_C and dc capacitor voltages v_{dck} in PHB with the proposed scheme under (a) $I_{Sm} = 18$ A, $v^*_{Cqm} = 0.2$ V, (b) $I_{Sm} = 30$ A, $v^*_{Cqm} = 0.2$ V, and (c) $I_{Sm} = 30$ A, $v^*_{Cqm} = 0.5$ V.

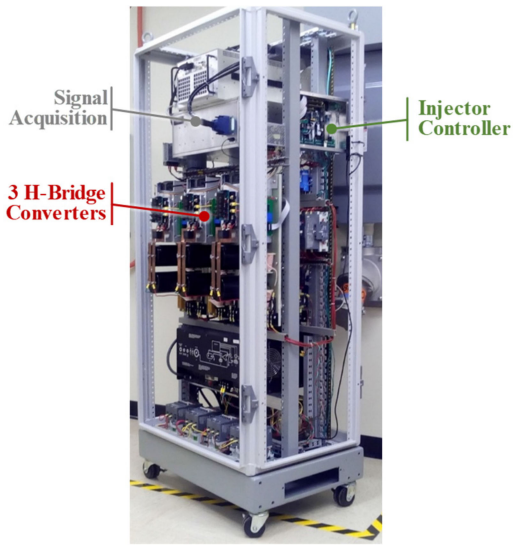

Fig. 13. Photograph of experimental impedance measurement setup prototype consisting of a series injector paralleling three H-bridge converters.

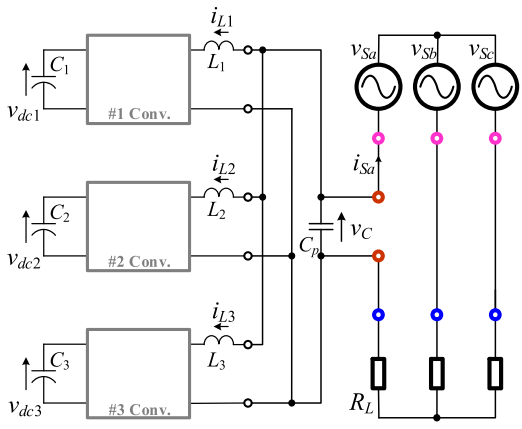

Fig. 14. Block diagram of the overall experimental test system.

The parameters of the PHB and the load subsystem are listed in Table II.

According to the parasitic parameters of devices used in the H-bridge converter, the critical point of the system current

TABLE II
PARAMETERS OF PHB-BASED SERIES INJECTOR AND LOAD SUBSYSTEM IN THE EXPERIMENTAL TEST SYSTEM

Symbol	Description	Value
C_k	DC capacitor	16.4 mF
L_k	AC inductor	0.66 mH
C_p	AC capacitor	66 μF
R_L	Load resistor	3 Ω
f_0	Fundamental frequency	60 Hz
f_s	Switching frequency	10 kHz
$v_{dc}{}^*$	DC voltage reference	130 V
v^*_{cqm}	Reference of reactive component magnitude in output voltage	2V

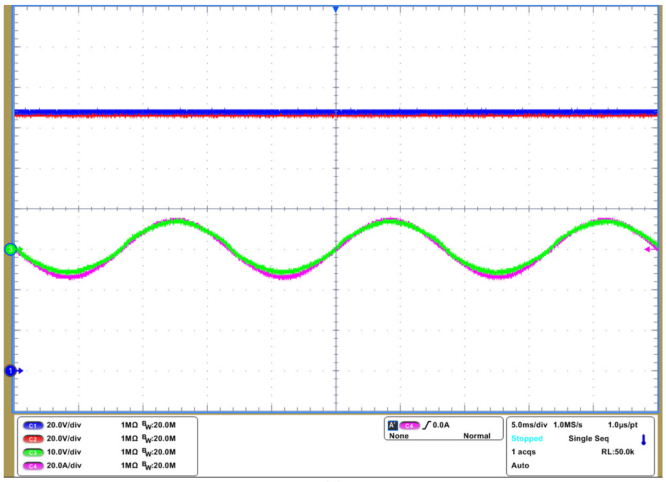

(a)

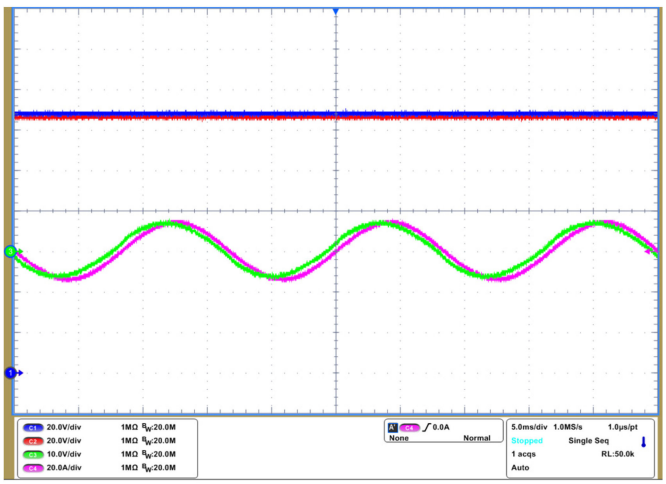

(b)

Fig. 15. Experimental waveforms of PHB-based series injector when $V_{Sm} = 40$ V, $v_p{}^* = 0$ V under (a) existing control scheme and (b) proposed control scheme: CH1, v_{dc1}, 20 V/div; CH2, v_{dc2}, 20 V/div; CH3, v_C, 10 V/div; CH4, i_{Sa}, 20 A/div; *t*, 5 ms/div.

magnitude I^C_{Sm} in the PHB with the existing scheme can be estimated, which is around 22 A. Therefore, the dc voltages will be imbalance in the PHB with the existing scheme when the system current magnitude exceeds 22 A. Fig. 15 shows the experimental results of the PHB with the existing scheme and proposed scheme under the source voltage magnitude of 40 V.

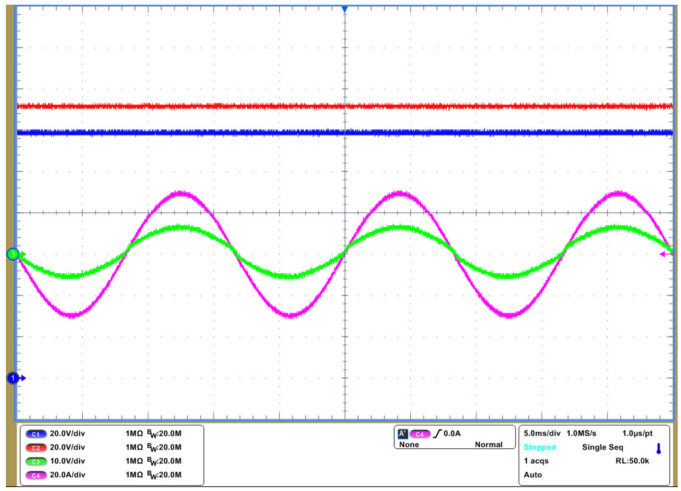

(a)

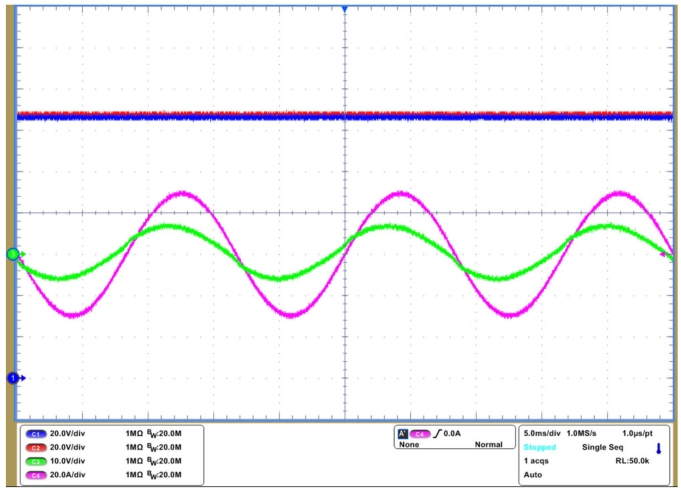

(b)

Fig. 16. Experimental waveforms of PHB-based series injector when $V_{Sm} = 80$ V, $v_p{}^* = 0$ V under (a) existing control scheme and (b) proposed control scheme: CH1, v_{dc1}, 20 V/div; CH2, v_{dc2}, 20 V/div; CH3, v_C, 10 V/div; CH4, i_{Sa}, 20 A/div; *t*, 5 ms/div.

It can be seen in Fig. 15(a) that dc voltages v_{dc1} and v_{dc2} are very close to their references of 130 V, and are balanced. In this case, the system current magnitude is 13.3 A, which is lower than its critical point, and thus dc voltages in the existing control scheme must be balanced based on the above analysis. The experimental waveforms in the PHB with the proposed scheme is shown in Fig. 15(b), and it can be found that output voltage leads system current since the reactive component is injected in output voltage. The dc voltages are also very close to their reference of 130 V and are balanced since the reference of reactive component magnitude is larger than its boundary.

Then the source magnitude is increased to 80 V, and the experimental test results are presented in Fig. 16. In Fig. 16(a), it can be seen that the difference between dc voltages v_{dc1} and v_{dc2} is around 12 V, and dc voltages are imbalance obviously. In this case, the system current magnitude is 26.7 A approximately, which is larger than its critical point, and the dc voltages must be imbalance since the positive feedback

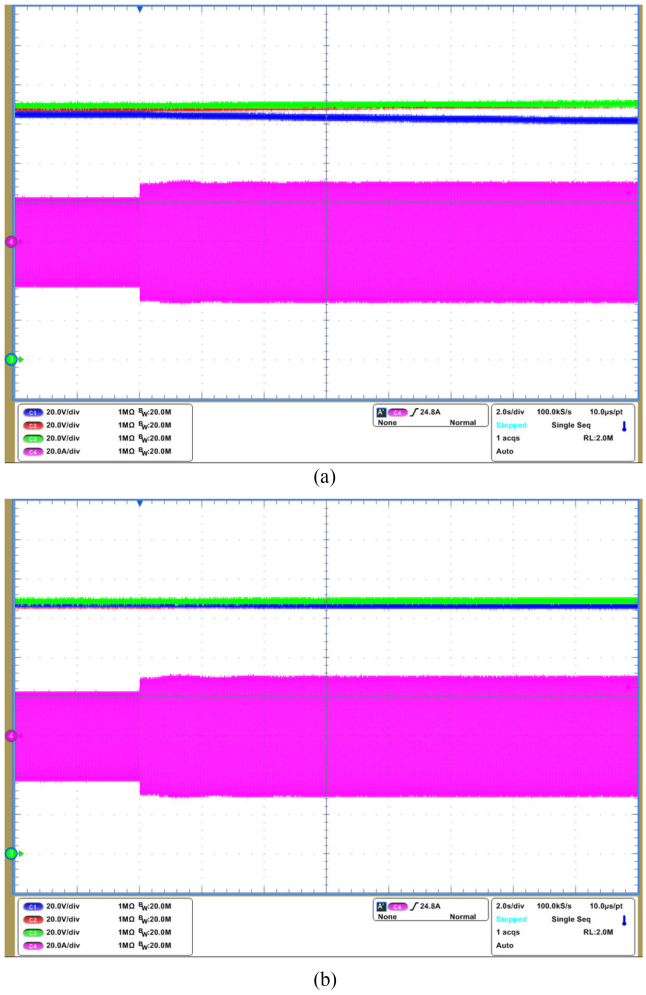

Fig. 17. Experimental waveforms of PHB-based series injector when source voltage magnitude is transited from 60 V to 80 V under (a) existing control scheme and (b) proposed control scheme: CH1, v_{dc1}, 20 V/div; CH2, v_{dc2}, 20 V/div; CH3, v_{dc3}, 20 V/div; CH4, i_{Sa}, 20 A/div; *t*, 2 s/div.

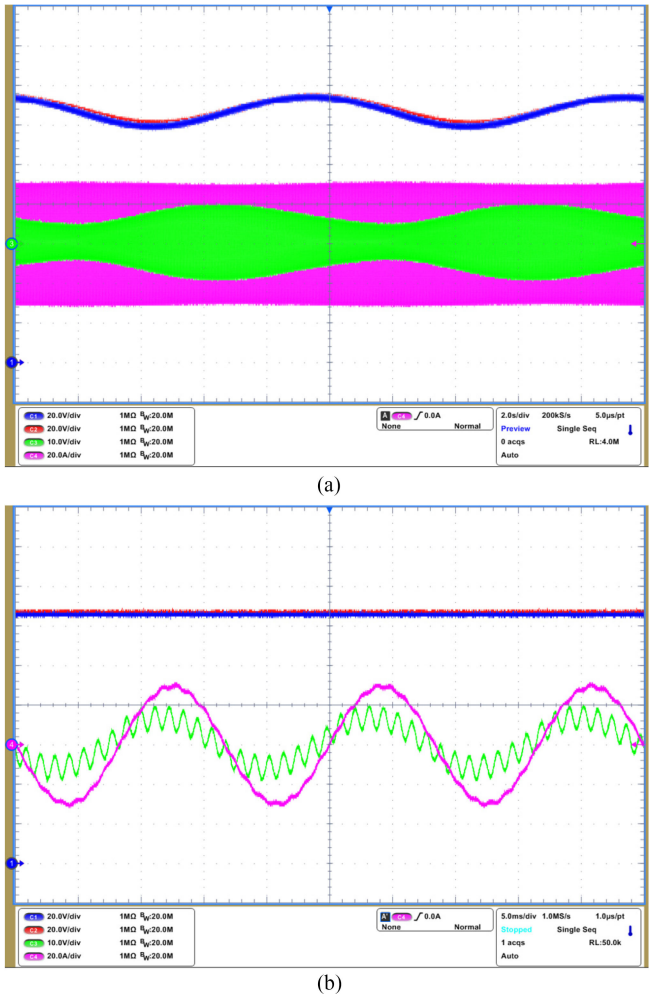

Fig. 18. Experimental waveforms of PHB-based series injector with the proposed scheme when $V_{Sm} = 80\,\text{V}$, $v^*_{pm} = 2\,\text{V}$ and (a) $f_p = 60.1\,\text{Hz}$ and (b) $f_p = 1060\,\text{Hz}$: CH1, v_{dc1}, 20 V/div; CH2, v_{dc2}, 20 V/div; CH3, v_C, 10 V/div; CH4, i_{Sa}, 20 A/div; *t*, (a) 2 s/div, (b) 5 ms/div.

happens in the dc voltage balancing loop. However, in Fig. 16(b) associated with the proposed scheme, dc voltages are still very close to their reference and balance. Therefore, the feasible of the proposed scheme for extending the operating range of the system current is verified.

Fig. 17 presents the waveforms of PHB with the existing scheme and proposed scheme when the source voltage magnitude V_{sm} is transited from 60 to 80 V. It can be seen in Fig. 17(a) that at beginning dc voltages are almost balanced, and then dc voltage v_{dc1} decreases while the other two dc voltages slightly increase as soon as the system current magnitude steps up. Since the system current magnitude steps from 20 to 26.7 A approximately, the dc voltage balancing loop transfers from negative feedback to positive feedback, and the dc voltage balancing is broken. In Fig. 17(b), dc voltages are always close to their reference during the step up transition of system current magnitude, and the robust of the proposed scheme is demonstrated. Besides, it can be observed in Figs. 15(b) and 16(b) that the phase angle between output voltage and system current φ_{VC} increases from 17° to 22° approximately while system current magnitude increases from 13.3 to 26.7 A, because the active component magnitude of the output voltage is reduced.

Fig. 18 shows the waveforms of the series injector injecting perturbation voltage into the system for measuring the impedance with the proposed scheme, where the perturbation voltage magnitude reference is set to 2 V. In Fig. 18(a), the perturbation frequency is 60.1 Hz for measuring the impedance at 0.1 Hz [9]. It can be seen that there are fluctuations of 0.1 Hz in dc voltages due to the interactions between the perturbation voltage and the inductor currents, while the dc voltages are always balanced during the fluctuation. In Fig. 18(b), the perturbation frequency is set to 1060 Hz for measuring the impedance at 1 kHz. It can be observed that dc voltages are balanced during the perturbation injection. Consequently, the feasibility of the proposed dc voltage balancing scheme for the series injector in ac impedance measurement application is demonstrated.

VII. Conclusion

A transformerless series injector based on PHB for ac impedance measurement is studied in this paper. The imbalance mechanism of dc voltages in the existing control scheme is analyzed, and it reveals that a positive feedback appears in the dc voltage balancing loop when the system current magnitude exceeds a critical point which is just determined by the power losses characteristics of H-bridge converter. Furthermore, an enhanced control scheme is proposed to make the PHB operate safely in full system current range by introducing both reactive components in output voltage and reactive circulating current among H-bridge converters for redistributing active power. It also proves that dc voltages of PHB can be balanced during full system current range with a properly designed reactive component magnitude of the output voltage in the proposed scheme.

The imbalance mechanism of dc voltages in the existing scheme and the feasibility of the proposed scheme are demonstrated by both simulation and experimental results. The proposed control scheme extends the system current capability of PHB and will be attractive in ac impedance measurement applications.

Appendix

The power losses of power semiconductor devices in the H-bridge converter are derived in this part.

First, the terminal voltage of the H-bridge v_{Bk} in Fig. 4 can be expressed in the following equation:

$$v_{Bk} = V_{Bkm}\sin\left(\varphi - \varphi_0\right). \tag{A.1}$$

Then the duty cycle of the diode D_1 and the IGBT T_2 can be obtained, which are presented in the following equations:

$$d_{D1} = \frac{1}{2} + \frac{V_{Bkm}}{2v_{dck}}\sin\left(\varphi - \varphi_0\right) \tag{A.2}$$

$$d_{T2} = \frac{1}{2} - \frac{V_{Bkm}}{2v_{dck}}\sin\left(\varphi - \varphi_0\right). \tag{A.3}$$

Thus the conduction losses and switching losses of the diode and IGBT are estimated based on the loss models of the devices shown in (9)–(13), and they are expressed as follows:

$$P_{con,D1} = \frac{1}{2\pi}\int_0^{\pi}\left(V_f + R_{ak}i_{Lk}\right)\cdot i_{Lk}\cdot d_{D1}\cdot d\varphi \tag{A.4}$$

$$P_{con,T2} = \frac{1}{2\pi}\int_0^{\pi}\left(V_t + R_{ce}i_{Lk}\right)\cdot i_{Lk}\cdot d_{T2}\cdot d\varphi \tag{A.5}$$

$$P_{sw,D1} = \frac{f_s}{2\pi}\int_0^{\pi} A_{rec}i_{Lk}\cdot\frac{v_{dck}}{V_{base}}\cdot d\varphi \tag{A.6}$$

$$P_{sw,T2} = \frac{f_s}{2\pi}\int_0^{\pi}\left(A_{on} + A_{off}\right)i_{Lk}\cdot\frac{v_{dck}}{V_{base}}\cdot d\varphi. \tag{A.7}$$

Finally, the total power losses of all diodes and IGBTs in H-bridge converter can be calculated by the following equation:

$$P_{Bk} = 4\cdot\left(P_{con,D1} + P_{con,T2} + P_{sw,D1} + P_{sw,T2}\right). \tag{A.8}$$

References

[1] J. Sun, "Small-Signal methods for AC distributed power systems—A review," *IEEE Trans. Power Electron.*, vol. 24, no. 11, pp. 2545–2554, Nov. 2009.

[2] D. Dong, B. Wen, D. Boroyevich, P. Mattavelli, and Y. Xue, "Analysis of phase-locked loop low-frequency stability in three-phase grid-connected power converters considering impedance interactions," *IEEE Trans. Ind. Electron.*, vol. 62, no. 1, pp. 310–321, Jan. 2015.

[3] R. Burgos, D. Boroyevich, F. Wang, K. Karim, and G. Francis, "AC stability of high power factor multi-pulse rectifiers," in *Proc. IEEE Energy Convers. Congress Expo.*, 2011, pp. 3758–3765.

[4] M. Belkhayat, "Stability criterion for AC power systems with regulated loads," Ph.D. dissertation, Purdue Univ., Lafayette, IN, USA, 1997.

[5] B. Wen, D. Boroyevich, R. Burgos, P. Mattavelli, and Z. Shen, "Small-signal stability analysis of three-phase AC systems in the presence of constant power loads based on measured d-q frame impedances," *IEEE Trans. Power Electron.*, vol. 30, no. 10, pp. 5952–5963, Oct. 2015.

[6] M. Cespedes and J. Sun, "Impedance modeling and analysis of grid-connected voltage-source converters," *IEEE Trans. Power Electron.*, vol. 29, no. 3, pp. 1254–1261, Mar. 2014.

[7] A. Rygg, M. Molinas, C. Zhang, and X. Cai, "A modified sequence-domain impedance definition and its equivalence to the dq-domain impedance definition for the stability analysis of AC power electronic systems," *IEEE J. Emerging Sel. Top. Power Electron.*, vol. 4, no. 4, pp. 1383–1396, Dec. 2016.

[8] Y. L. Familiant, K. A. Corzine, J. Huang, and M. Belkhayat, "AC impedance measurement techniques," in *Proc. IEEE Int. Conf. Elect. Mach. Drives*, 2005, pp. 1850–1857.

[9] H. Jing, K. A. Corzine, and M. Belkhayat, "Small-Signal impedance measurement of power-electronics-based AC power systems using Line-to-Line current injection," *IEEE Trans. Power Electron.*, vol. 24, no. 2, pp. 445–455, Feb. 2009.

[10] G. Francis, R. Burgos, D. Boroyevich, F. Wang, and K. Karimi, "An algorithm and implementation system for measuring impedance in the D-Q domain," in *Proc. IEEE Energy Convers. Congress Expo.*, 2011, pp. 3221–3228.

[11] Y. A. Familiant, H. Jing, K. A. Corzine, and M. Belkhayat, "New techniques for measuring impedance characteristics of three-phase AC power systems," *IEEE Trans. Power Electron.*, vol. 24, no. 7, pp. 1802–1810, Sep. 2009.

[12] Z. Shen, M. Jakšić, P. Mattavelli, D. Boroyevich, J. Verhulst, and M. Belkhayat, "Design and implementation of three-phase AC impedance measurement unit (IMU) with series and shunt injection," in *Proc. IEEE Appl. Power Electron. Conf. Expo.*, 2013, pp. 2674–2681.

[13] M. Jakšić, Z. Shen, I. Cvetkovic, D. Boroyevich, R. Burgos, and P. Mattavelli, "Multi-level single-phase shunt current injection converter used in small-signal dq impedance identification," in *Proc. IEEE Appl. Power Electron. Conf. Expo.*, 2014, pp. 2775–2782.

[14] M. Jakšić, D. Boroyevich, R. Burgos, Z. Shen, I. Cvetkovic, and P. Mattavelli, "Modular interleaved single-phase series voltage injection converter used in small-signal dq impedance identification," in *Proc. IEEE Energy Convers. Congress Expo.*, 2014, pp. 3036–3045.

[15] M. Jakšić *et al.*, "Medium-Voltage impedance measurement unit for assessing the system stability of electric ships," *IEEE Trans. Energy Conversion*, vol. 32, no. 2, pp. 829–841, Jun. 2017.

[16] M. Ciobotaru, R. Teodorescu, and F. Blaabjerg, "A new single-phase PLL structure based on second order generalized integrator," in *Proc. IEEE Power Electron. Specialists Conf.*, 2006, pp. 1–6.

[17] S. Rodrigues, A. Papadopoulos, E. Kontos, T. Todorcevic, and P. Bauer, "Steady-State loss model of half-bridge modular multilevel converters," *IEEE Trans. Ind. Appl.*, vol. 52, no. 3, pp. 2415–2425, May/Jun. 2016.

[18] W. Hurley and W. Wolfle, *Transformers and Inductors for Power Electronics: Theory, Design and Applications*. Hoboken, NJ, USA: Wiley, 2013.

[19] S. Dieckerhoff, S. Bernet, and D. Krug, "Power loss-oriented evaluation of high voltage IGBTs and multilevel converters in transformerless traction applications," *IEEE Trans. Power Electron.*, vol. 20, no. 6, pp. 1328–1336, Nov. 2005.

[20] K. Ma, A. S. Bahman, S. Beczkowski, and F. Blaabjerg, "Complete loss and thermal model of power semiconductors including device rating information," *IEEE Trans. Power Electron.*, vol. 30, no. 5, pp. 2556–2569, May 2015.

Zeng Liu (S'09–M'14) received the B.S. degree from Hunan University, Changsha, China, and the M.S. and Ph.D. degrees from Xi'an Jiaotong University (XJTU), Xi'an, China, in 2006, 2009, and 2013, respectively, all in electrical engineering.

He then joined XJTU as a Faculty Member in electrical engineering, where he is currently an Associate Professor. From 2015 to 2017, he was with the Center for Power Electronics Systems, Virginia Polytechnic Institute and State University, Blacksburg, VA, USA, as a Visiting Scholar. His research interests include control of parallel inverters, transfer control of grid-tied inverters, and small-signal stability of three-phase ac power electronics systems.

Igor Cvetkovic (S'10–M'17) received the Dipl. Ing. degree from the University of Belgrade, Belgrade, Serbia, in 2004, and the M.S. and Ph.D. degrees from Virginia Polytechnic Institute and State University (Virginia Tech), Blacksburg, VA, USA, in 2010 and 2017, respectively.

From 2004 to 2007, he was with the Electric Power Industry of Serbia as an Engineer. In 2010, he joined the Center of Power Electronics Systems, Virginia Tech, as a Research Engineer, where he currently is a Research Scientist and a Technical Director. His research interests include ac- and dc- electronic power distribution systems design and stability, as well as power electronics-based system-level modeling and control.

Zhiyu Shen (S'11–M'13) received the B.S. and M.S. degrees in electrical engineering from Tsinghua University, Beijing, China, and Ph.D. degree in electrical engineering from Virginia Tech, Blacksburg, VA, USA, in 2004, 2007, and 2013, respectively.

After graduation, he worked as a Research Scientist with the Center for Power Electronics System, Virginia Tech until 2016. From 2016 to 2018, he worked with General Electric Global Research as a Lead Power Electronics Engineer. In 2018, he joined Delta Electronics (America) as a member of R&D staff with Delta Power Electronics Laboratory. His research interests include three-phase ac system impedance measurement, three-phase ac system small signal stability, high-frequency high-density converter design, and control system architecture in high power converters.

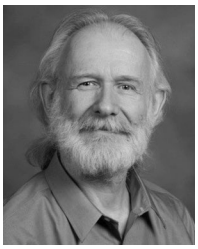

Dushan Boroyevich (S'81–M'86–SM'03–F'06) received the Dipl. Ing. degree from the University of Belgrade, Belgrade, Serbia, in 1976, and the M.S. degree from the University of Novi Sad, Novi Sad, Serbia, in 1982, in what then used to be Yugoslavia. He received the Ph.D. degree from Virginia Polytechnic Institute and State University (Virginia Tech), Blacksburg, VA, USA, in 1986.

From 1986 to 1990, he was an Assistant Professor and Director with the Power and Industrial Electronics Research Program, the Institute for Power and Electronic Engineering, the University of Novi Sad. He then joined the Bradley Department of Electrical and Computer Engineering, Virginia Tech as an Associate Professor. He is currently the University Distinguished Professor with the department and Director with the Center for Power Electronics Systems. He was the President of the IEEE Power Electronics Society for 2011–12. His research interests include electronic energy systems, multiphase power conversion, power electronics systems modeling and control, and integrated design of power converters.

Dr. Boroyevich is a member of the US National Academy of Engineering and is recipient of numerous awards, including the IEEE William E. Newell Power Electronics Technical Field Award and the European Power Electronics Association Outstanding Achievement Award.

Rolando Burgos (S'96–M'03) received the B.S. in electronics engineering, the electronics engineering professional degree, and the M.S. and Ph.D. degrees in electrical engineering from the University of Concepción, Chile, in 1995, 1997, 1999, and 2002, respectively.

In 2002, he joined, as a Postdoctoral Fellow, the Center for Power Electronics Systems (CPES), Virginia Tech, Blacksburg, VA, USA, becoming Research Scientist in 2003, and Research Assistant Professor, in 2005. In 2009, he joined ABB Corporate Research in Raleigh, NC, USA, where he was a Scientist (2009–2010), and Principal Scientist (2010–2012). In 2010, he was appointed Adjunct Associate Professor with the Electrical and Computer Engineering Department, North Carolina State University, the Future Renewable Electric Energy Delivery and Management Systems Center. In 2012, he returned to Virginia Tech where he is currently Associate Professor with The Bradley Department of Electrical and Computer Engineering, CPES Faculty, and member of the CPES Executive Board. His research interests include wide-bandgap semiconductor-based power conversion, packaging and integration, electromagnetic interference and electromagnetic compatibility, multi-phase multi-level power converters, grid power electronics systems, stability of ac and dc power systems, and modeling and control of power electronics converters and systems.

Dr. Burgos is member of the IEEE Power Electronics Society where he currently serves Chair of the Power and Control Core Technologies Committee, as an Associate Editor of the IEEE TRANSACTIONS ON POWER ELECTRONICS, IEEE POWER ELECTRONICS LETTERS, and the IEEE JOURNAL OF EMERGING AND SELECTED TOPICS IN POWER ELECTRONICS. He is also a member of the IEEE Industry Applications Society, the IEEE Industrial Electronics Society, and the IEEE Power and Energy Society.

Jinjun Liu (M'97–SM'10–F'19) received the B.S. and Ph.D. degrees in electrical engineering from Xi'an Jiaotong University (XJTU), Xi'an, China, in 1992 and 1997, respectively.

He then joined the XJTU Electrical Engineering School as a Faculty. From late 1999 to early 2002, he was with the Center for Power Electronics Systems, Virginia Polytechnic Institute and State University, Blacksburg, VA, USA, as a Visiting Scholar. In late 2002, he was promoted to a Full Professor and then the Head of the Power Electronics and Renewable Energy Center, XJTU, which now comprises 16 faculty members and more than 100 graduate students and carries one of the leading power electronics programs in China. From 2005 to early 2010, he served as an Associate Dean with the Electrical Engineering School, XJTU, and from 2009 to early 2015, the Dean for Undergraduate Education of XJTU. He is currently a XJTU Distinguished Professor of Power Electronics, sponsored by Chang Jiang Scholars Program of Chinese Ministry of Education. He coauthored 3 books (including one textbook), authored or coauthored more than 400 technical papers in peer-reviewed journals and conference proceedings, holds 42 invention patents (China/US), and delivered for many times plenary keynote speeches and tutorials at IEEE conferences or China national conferences in power electronics area. His research interests include power quality control and utility applications of power electronics, microgrids for sustainable energy and distributed generation, and more/all electronic power systems.

Dr. Liu was the recipient of eight times governmental awards at national level or provincial/ministerial level for scientific research achievements or academic/teaching career achievements. He also received the 2006 Delta Scholar Award, the 2014 Chang Jiang Scholar Award, the 2014 Outstanding Sci-Tech Worker of the Nation Award, and the IEEE TRANSACTIONS ON POWER ELECTRONICS 2016 Prize Paper Award. He served as the IEEE Power Electronics Society Region 10 Liaison and then China Liaison for 10 years, an Associate Editor for the IEEE TRANSACTIONS ON POWER ELECTRONICS for 12 years, and from starting 2015, the Vice President for membership of IEEE PELS. He is on the Board of China Electrotechnical Society and was elected the Vice President of the CES Power Electronics Society in 2013. Since 2013, he has been the Vice President for International Affairs, China Power Supply Society (CPSS) and since 2016, the inaugural Editor-in-Chief of CPSS Transactions on Power Electronics and Applications. Since 2013, he has been serving as the Vice Chair of the Chinese National Steering Committee for College Electric Power Engineering Programs.